On the Generator Constraint Design of a Wave Energy Converter at a Pre-Sizing Stage

Sébastien Olaya, Jean-Matthieu Bourgeot, Mohamed Benbouzid

On the Generator Constraint Design of a Wave Energy Converter at a Pre-Sizing Stage

Sébastien OLAYA*‡, Jean-Matthieu BOURGEOT*‡ and Mohamed El-Hachemi BENBOUZID†‡
*École Nationale d'Ingénieurs de Brest (ENIB)
olaya@enib.fr, bourgeot@enib.fr
†Université de Bretagne Occidentale (UBO)
Mohamed.Benbouzid@univ-brest.fr
‡Laboratoire Brestois de Mécanique et des Systèmes - EA4325 LBMS

***Abstract*—This paper deals with the constraint pre-design of the energy conversion chain for a wave energy converter application. At the first step, and because the control input is the torque (or the linear force) delivered by the generator, we start by limiting mechanically the nominal velocity. For that purpose, we introduce a new quantity based on short-term wave analysis, namely the maximum expected relative velocity. It may be evaluated when both the wave energy converter is controlled or not. Using long-term wave analysis, based on a known local wave climate, we can constraint the maximum relative velocity that the system have to handle. It appears that because of the constraint applied on the torque, it has to be chosen when no loading is applied. Once it have been chosen, we can then determine the generator nominal power rating based on a time-domain analysis. In this context we use two simple criteria *(i)* one based on the maximisation of the produced electrical energy, *(ii)* the second on the maximisation of the annual profit. From numerical investigation, it appears that it exists a point which make a compromise between these two antinomic criteria.**

***Index Terms*—Wave energy converter, self-reacting point absorber, optimal control, generator constraint, pre-design.**

I. Introduction

WAVE energy conversion represents a huge potential in term of renewable energy resource and receives more and more attention from many developers around the world although it still remains immature compared to other renewable technologies [1]. Many working principles, with different power take-off (PTO) concepts, have emerged during the past century [2]. In order to be economically efficient, it is also now well established that, wave energy converter has to be controlled. However whatever will be the control strategy, one important thing to keep in mind is that a real system have physical limits. Then the proposed control strategy will have to deal with.

Recent approach proposed to formulate the energy absorption problem as an optimisation problem and then those physical limits can easily be handled; see for example [3]–[5] for a single WEC and [6] for a two-body WEC. The main question, now, is to decide which variables has to be constrained in control formulation and how to fix the limits in a realistic fashion? To the best knowledge of the authors only few references in the literature considered this problem or part of it [7], [8], but it is not really explained how to fix the limits. In this paper we will follow a similar approach that the one presented in [9], where the authors applied global considerations (power limitation requirement, energy potential, control strategy) in the design process of a marine current turbine.

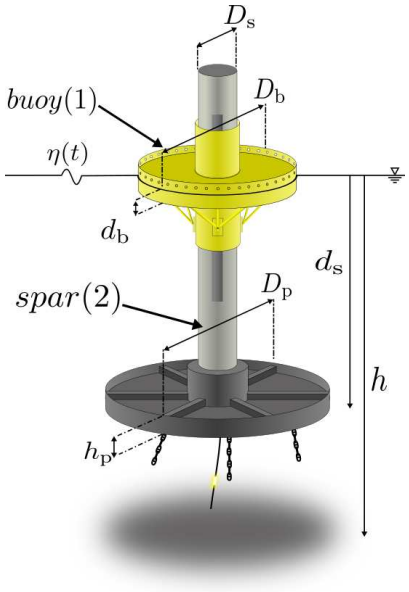

Fig. 1: Sketch of a generic self-reacting point absorber.

Obviously energy conversion chain constraints are mainly due to the actuator limits in term of nominal torque, nominal velocity and nominal generator power rating. Also we have to keep in mind that, if considering a linear generator, $P_{\mathrm{nom}} = f_{\mathrm{gen,nom}} \times v_{\mathrm{r,nom}}$ and then, fixing two of the parameters, will fix the third one. As a general remark, and because most of the time authors impose constraints on the nominal power rating, we have to mention that $f_{\mathrm{gen,nom}}$ and $v_{\mathrm{r,nom}}$ are the real limit values imposed by the power electronics conversion system. They must not be overshooted.

In the following, Section II present the mathematical modelling necessary background for a generic self-reacting point absorber. By generic, we mean that we do not make any assumptions on the PTO working principle. Section III reminds some concepts regarding optimal control using model predictive strategy. Section IV explain how to fix the generator nominal velocity after having reminded some practical aspects short- and long-term wave analysis. Then, we introduce two antinomic criteria in Section V that allowed us to constraint the nominal power rating. Sections IV and V are illustrated with numerical examples for which we consider a generic self-reacting point absorber as the one depicted on Fig. 1 with a working principle and dimensions similar to the PB150 from Ocean Power Technology [10]. Main used dimensions and

TABLE I: WEC Geometric Input Parameters

Parameters	Symbol	Value	Units
Buoy draft	d_b	1.5	[m]
Buoy outer diameter	D_b	9.5	[m]
Plate diameter	D_p	11.8	[m]
Plate height	h_p	1.5	[m]
Spar diameter	D_s	3	[m]
Spar draft	d_s	35	[m]

parameters are given in TABLE I.

II. Mathematical Modelling

In this section we present the mathematical formulation of the linearised model for a generic self-reacting WEC. For the sake of simplicity, the total structure dynamics is restricted to the heaving mode. Under the assumption of linear wave potential theory, the linearised motion equation for the two bodies is given by the Newton's second law. In what follows, indices 1 is used for what is refereed to the buoy and 2 to the spar.

$$\begin{cases} m_1\ddot{z}_1 = f_{\mathrm{ex},1} + f_{\mathrm{r},11} + f_{\mathrm{r},21} + f_\mathrm{gen} + f_{\mathrm{s},1} \\ m_2\ddot{z}_2 = f_{\mathrm{ex},2} + f_{\mathrm{r},22} + f_{\mathrm{r},12} - f_\mathrm{gen} + f_{\mathrm{s},2} + f_\mathrm{drag} \end{cases} \tag{1}$$

where m_1 and m_2 are respectively the buoy and the spar mass, z_i is the body i vertical displacement with respect to the equilibrium position. $f_{\mathrm{ex},i}$ is the wave excitation force applied on body i. It can be expressed in the time-domain as

$$f_{\mathrm{ex},i}(t) = \int_{-\infty}^{\infty} h_{\mathrm{ex},i}(t-\tau)\eta_\mathrm{o}(\tau)\mathrm{d}\tau \tag{2}$$

where $\eta_\mathrm{o}(t)$ is the wave elevation due to the incident wave at the origin O, located at the intersection of the undisturbed free surface level with cylinder axis and $h_{\mathrm{ex},i}(t)$ is the impulse response of the wave excitation force related to the geometry of the body i [11]. $f_{\mathrm{r},ij}$ is the force applied on the body j due to the motion of body i. This force is associated to the radiation problem. In linear potential theory, it is conventional to decompose this force in two parts which are frequency dependent. One is proportional to the body acceleration, the other is proportional to its velocity and they are respectively referenced as the added mass and radiation damping.

$$f_{\mathrm{r},ij} = -m_{\mathrm{a},ij}(\omega)\ddot{z}_i(t) - b_{ij}(\omega)\dot{z}_i(t) \tag{3}$$

Because of the hydrodynamic coefficient frequency dependence, it is convenient to replace (3) by an easiest computational formulation. Cummins [12] shown that it can be approximated by the following representation in the time-domain for the zero forward speed case

$$f_{\mathrm{r},ij} = -m_{\mathrm{a},ij}(\infty) - \int_{-\infty}^{t} k_{ij}(t-\tau)\dot{z}_i(\tau)\mathrm{d}\tau \tag{4}$$

where $m_{\mathrm{a},ij}(\infty)$ is defined as the infinite added mass and $k_{ij}(t)$ is the radiation convolution kernel. $f_{\mathrm{s},i}$ is the net restoring force due to gravity and buoyancy which is proportional to the displacement of the body structure from its equilibrium position. The coefficient of proportionality is denoted $\kappa_{\mathrm{s},i}$ and is referenced as the buoyancy stiffness

$$f_{\mathrm{s},i}(t) = -\kappa_{\mathrm{s},i} z_i(t) \tag{5}$$

where the diagonal elements are respectively defined for the buoy and the platform by $\kappa_{\mathrm{s},1}$ and $\kappa_{\mathrm{s},2}$ such as

$$\kappa_{\mathrm{s},i} = \rho g \iint\limits_{S_{\mathrm{F0},i}} \mathrm{d}S \tag{6}$$

where ρ is the water density, g is the gravitational acceleration and $S_{\mathrm{F0},i}$ is the water plane area at equilibrium condition. In the cylindrical shape case, we have $\kappa_{\mathrm{s},1} = \rho g \frac{\pi}{4}(D_\mathrm{b}^2 - D_\mathrm{s}^2)$ for the buoy and $\kappa_{\mathrm{s},2} = \rho g \frac{\pi}{4} D_\mathrm{s}^2$ for the spar.

In order to enhance the spar modelling during the resonant oscillation and in view of its geometry i.e. a damping plate with sharp edges attached at the column bottom, it is convenient to introduce an additional non-linear drag force where the drag term is proportional to the square of the velocity and expressed as

$$f_\mathrm{drag} = -\frac{1}{2}\rho S_\mathrm{p} C_\mathrm{d}\dot{z}_2|\dot{z}_2| \tag{7}$$

where S_p is the cross sectional area of the plate normal to the displacement, C_d is the drag coefficient. The latest coefficient have to be experimentally determined based on measurement for different forcing amplitudes and frequencies. More details on the non-linear term influence and treatment can be found in [13]. However in this paper rather than using a non-linear drag term, we use, as a first approximation, a constant linear damping term b_drag, proportional to the spar velocity such as $f_\mathrm{drag} = -b_\mathrm{drag}\dot{z}_2$. In this paper the additional damping is chosen in such a way that it corresponds to the maximum dissipation of the non-linear term when optimal active control is applied[1] which corresponds approximatively, after numerical investigation, to 14.5% of the critical damping defined as $b_{\mathrm{crit},2} = 2\sqrt{(m_2 + m_{\mathrm{a},22}(\infty))\kappa_2}$. Finally, f_gen denotes the force due to the generator which is also the control input.

Based on the above development and using a matrix notation, the equation system (1) can be rewrite as

$$\begin{aligned}(\mathrm{M} + \mathrm{M_a}(\infty))\ddot{\xi}(t) + \int_{-\infty}^{t} \mathrm{K}(t-\tau)\dot{\xi}(\tau)\mathrm{d}\tau \\ + \mathrm{B_{drag}}\dot{\xi}(t) + \mathrm{K_s}\xi(t) = F_\mathrm{ex}(t) + F_\mathrm{gen}(t)\end{aligned} \tag{8}$$

where $\xi = \begin{bmatrix} z_1 & z_2 \end{bmatrix}^T$. This integro-differential equation is referenced in the literature as the Cummins formulation. It is well established in the wave energy community that direct computation of (8), based on a discrete-time approximation, is not efficient and is not appropriated for control purposes. The use of parametric models based on a state-space representation that approximate the convolution kernels (2) and (4) are more suitable. In [14], authors provide a MATLAB toolbox which approximate the convolution terms of (4) by a linear time-invariant system. Regarding the wave excitation forces, Falnes in [15], shown that the convolution kernel $h_{\mathrm{ex},i}(t)$ of (2) is not necessary causal because of the mathematical assumptions made for the hydrodynamic parameter determination. So, before identification, we have to make it causal, more details for the two-body WEC case can be found in [13].

Hydrodynamic coefficients, i.e. added mass, radiation damping, and wave excitation force, that are required in the identification process, are computed in the frequency-domain by a semi-analytical method described in [16].

III. Optimal Control Strategy Formulation

In this section we give to the reader some key elements regarding optimal control strategy, both in the frequency- and time-domain, applied to a self-reacting point absorber. All

[1]Optimal active impedance is found in the frequency-domain by numerical exhaustive search based on the non-linear model.

the following contents is part of a previous work which has already been published in [6].

The first step in formulating optimal control strategy when a multi-body wave energy converter is used such as the one depicted on Fig. 1 is to formulate what is called a phenomenologically one-body equivalent model [6], [17]. This latter is obtained in the frequency-domain, assuming linear wave potential theory, and applying Thévenin theorem on a electrical equivalent circuit. This equivalent model express the relative velocity $\hat{v}_\mathrm{r}$ in term of an equivalent intrinsic mechanical impedance $Z_\mathrm{i,eq}$, an equivalent wave excitation force $\hat{f}_\mathrm{ex,eq}$ and a linear force $\hat{f}_\mathrm{gen}$ describing the force due to the generator.

$$\hat{v}_\mathrm{r} = \frac{1}{Z_\mathrm{i,eq}}(\hat{f}_\mathrm{ex,eq} + \hat{f}_\mathrm{gen}) \tag{9}$$

From this equivalent model we can identify

- the maximum absorbed power, obtained when applying reactive control strategy and no constraints are considered. Assuming that $\hat{f}_\mathrm{gen} = Z_\mathrm{gen} \times \hat{v}_\mathrm{r}$, then reactive control strategy is obtained when[2] $Z_\mathrm{gen} = {Z_\mathrm{i,eq}}^*$ [17], [18]. This point is quite useful for discussing optimal performance in irregular wave when no constraints are considered.
- a lower order equivalent time-domain model defining the equivalent wave excitation force to relative velocity relation such as

$$v_\mathrm{r}(t) = \int_{-\infty}^{\infty} h(t-\tau)(u(\tau) + w(\tau))\mathrm{d}\tau \tag{10}$$

where $h(t) = \mathcal{F}^{-1}\{{Z_\mathrm{i,eq}}^{-1}(\mathrm{i}\omega)\}$, $u(t) \equiv f_\mathrm{gen}(t)$ and $w(t)$ is the equivalent wave excitation force in the time-domain defined as

$$w(t) = \int_0^{t+t_\mathrm{c}} g^{(\mathrm{c})}(t-\tau)\eta_\mathrm{o}(\tau + t_\mathrm{c})\mathrm{d}\tau \tag{11}$$

where $g(t)$ is the inverse Fourier transform of $G(\mathrm{i}\omega) \equiv \hat{f}_\mathrm{ex,eq}(\mathrm{i}\omega)$ and $g^{(c)}(t)$ its causal version [15], [19]

$$g(t) = \frac{1}{2\pi}\int_{-\infty}^{\infty} G(\mathrm{i}\omega)\exp^{-\mathrm{i}\omega t}\,\mathrm{d}\omega \tag{12}$$

Once the identification process has been performed, the obtained model that relates the force to relative velocity transfer is used for formulating an optimal control strategy based on model predictive control theory. Indeed, it can be shown that the absorbed energy maximization problem may be re-written as a quadratic optimisation problem subject to input constraints. This latter is solved in a receding horizon fashion using a Rosen's gradient projection method as QP solver. The whole procedure require the estimation and prediction of the equivalent wave excitation force. Because this latter point is still an open problem in the wave energy community, in what follows we will assume that we are able to provide the required entry to the QP solver. Figure 2 illustrates the applied control strategy.

IV. Maximum Relative Velocity Pre-Constraint

A. Short-term stochastic wave analysis

Content of this section is mainly based on Molin [20] and reader who is interested by details is referred to it. In what

[2]where * notation denotes complex conjugate

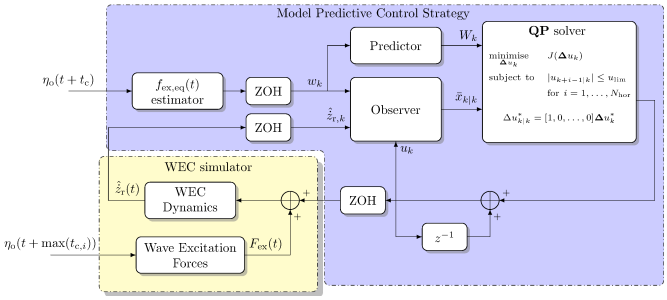

Fig. 2: Model predictive control strategy.

follows, we assume that irregular surface wave elevation is given by the simplest random wave model

$$\eta(t) = \sum_i A_i \cos(\omega_i t + \varphi_i) \tag{13}$$

where amplitude coefficients A_i are obtained from spectral description of the sea-state $S(\omega)$ such as

$$A_i^2 = 2S(\omega_i)\Delta\omega_i \tag{14}$$

and the random phases φ_i are uniformly distributed between 0 and 2π using a centered normal distribution. In this study we will consider a JONSWAP spectrum parametrised by a significant wave height H_s and a spectral peak wave period T_p.

$$S(\omega) = \alpha H_\mathrm{s}^2 \omega_\mathrm{p}\omega^{-5}\mathrm{e}^{-\frac{5}{4}(\frac{\omega}{\omega_\mathrm{p}})^{-4}}\gamma_\mathrm{J}^a \tag{15}$$

where

$$a = \mathrm{e}^{-\frac{(\omega-\omega_\mathrm{p})^2}{2\sigma^2\omega_\mathrm{p}^2}} \tag{16}$$

$\sigma = .07$ for $\omega < \omega_\mathrm{p}$ and $\sigma = .09$ for $\omega > \omega_\mathrm{p}$ and finally α have to be choosen in such a way as to ensure

$$H_\mathrm{s}^2 = 16\int_0^{\infty} S(\omega)\mathrm{d}\omega \tag{17}$$

In what follows we will consider a peak enhancement factor $\gamma_\mathrm{J} = 3.3$. According to Molin [20], it seems that it is realistic to assume that the maxima repartition follows a Rayleigh distribution. Considering a 3h time windows length T, for which we assume a stationary sea-state, it can be shown that the maximum expected amplitude $\bar{X}_\mathrm{Max}$ of a signal $X(t)$ that is linearly linked to the sea-state spectrum $S(\omega)$ can be expressed such as

$$\bar{X}_\mathrm{Max} = \left[\sqrt{2\ln\left(\frac{T}{T_\mathrm{z}}\right)} + \frac{\gamma}{\sqrt{2\ln\left(\frac{T}{T_\mathrm{z}}\right)}}\right]\sqrt{m_0} \tag{18}$$

where $\gamma = .5772$ is the Euler's constant. The mean zero up-crossing period T_z of the signal $X(t)$ is obtained from

$$T_\mathrm{z} = 2\pi\sqrt{\frac{m_0}{m_2}} \tag{19}$$

where its $n-\mathrm{th}$ spectral moment is defined as

$$m_n = \int_0^{\infty} \omega^n S_X(\omega)\mathrm{d}\omega \tag{20}$$

which is related to the spectral density S_X.

Based on all those definitions we are able to define a new quantity called the maximum expected relative velocity $\bar{v}_\mathrm{r,Max}$. This quantity is the maximum expected amplitude for

the relative velocity $v_{\mathrm{r}}(t)$, that should appear on the PTO when control strategy is applied and if no constraints on maximum values are considered. In the case where no control is applied we will use the notation $\bar{v}_{\mathrm{r},0}$.

In complex notation, the relative velocity $v_{\mathrm{r}}(t)$ can be expressed as

$$v_{\mathrm{r}}(t) = \frac{1}{2}\left(\hat{v}_{\mathrm{r}}\mathrm{e}^{-\mathrm{i}\omega t} + \hat{v}_{\mathrm{r}}^{*}\mathrm{e}^{\mathrm{i}\omega t}\right) \tag{21}$$

After some algebraic manipulations, we can show that the expected value $\mathrm{E}\left\{X(t)X^{*}(t+\tau)\right\}$ of the random variable, which is also defined as the autocorrelation signal $\mathrm{R}(\tau)$, can be expressed as

$$\mathrm{R}(\tau) = \sum_{i} \frac{1}{2} A_i^2 \left|\hat{v}_{\mathrm{r}}(\omega_i)\right|^2 \cos(\omega_i \tau) \tag{22}$$

Remembering that the irregular wave amplitude A_i is related to the wave spectrum $S(\omega)$ with (14), the previous equation can easily be transformed as

$$\mathrm{R}(\tau) = \sum_{i} S(\omega_i) \left|\hat{v}_{\mathrm{r}}(\omega_i)\right|^2 \cos(\omega_i \tau)\Delta\omega_i \tag{23}$$

Also because the autocorrelation $\mathrm{R}(\tau)$ is related to the one-sided spectral density such as

$$\mathrm{R}(\tau) = \int_0^{\infty} S_X(\omega)\cos(\omega\tau)\mathrm{d}\omega \tag{24}$$

we can identify $S_X(\omega)$ by comparison

$$S_X(\omega) = S(\omega)\left|\hat{v}_{\mathrm{r}}(\omega)\right|^2 \tag{25}$$

and then estimate the maximum expected amplitude $\bar{v}_{\mathrm{r,Max}}$ or $\bar{v}_{\mathrm{r},0}$ from (18), (19), and (20).

In a similar manner we could estimate the maximum expected generator force $\bar{f}_{\mathrm{gen,Max}}$ that should appeared on the PTO, if control strategy is linear, considering

$$S_X(\omega) = S(\omega)\left|Z_{\mathrm{gen}}\right|^2\left|\hat{v}_{\mathrm{r}}(\omega)\right|^2 \tag{26}$$

where Z_{gen} is the generator impedance.

Figures 3, 4 and, 5 illustrate maximum expected amplitude estimation respectively when the system is uncontrolled and when both passive and reactive control strategy are applied. For this numerical illustration we have considered a JONSWAP spectrum defined by a significant wave height $H_{\mathrm{s}} = 3\mathrm{m}$ and a spectrum peak period $T_{\mathrm{p}} = 8.5\mathrm{s}$. An approximatively one and half hour simulation time have been used in order to let the maximum amplitudes appearing. For passive control we have considered a constant damping coefficient such as $f_{\mathrm{gen}}(t) = -\beta_{\mathrm{gen}} v_{\mathrm{r}}(t)$. The damping coefficient have been chosen in order to maximize the harnessed energy at the considered spectrum, $\beta_{\mathrm{gen}} = 2\mathrm{e}^{6}\mathrm{N.s/m}$. Figures 6 and 7 shows estimation of the relative velocity and generator loading when both passive loading and MPC strategy are applied with no constraints and for several sea-states.

From numerical results it appears that equation (18) provides a good estimation of maximum expected relative velocity and generator loading for all the considered case study. Also one can notice that for this wave spectrum, maximum expected relative velocity is much higher when the system is not controlled rather than when passive loading is applied and equivalently the same when the optimal controller is used.

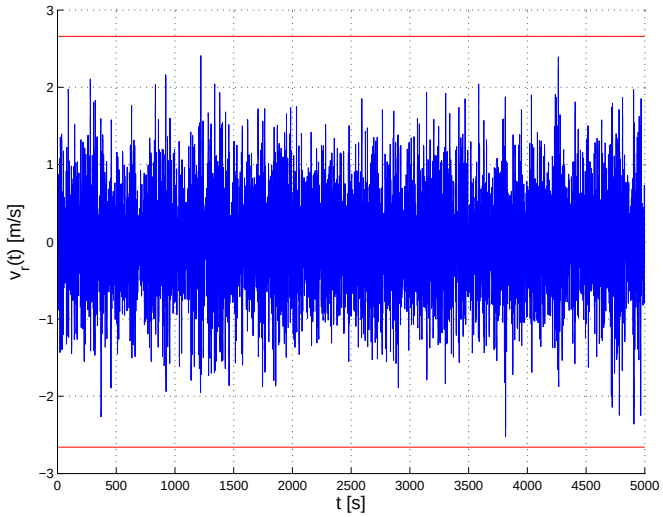

Fig. 3: Relative velocity $v_{\mathrm{r}}(t)$ time series representation when the system is uncontrolled and for a JONSWAP spectrum defined by $H_{\mathrm{s}} = 3\mathrm{m}$ and $T_{\mathrm{p}} = 8.5\mathrm{s}$. Maximum expected amplitude are drawn in red solid lines, $\bar{v}_{\mathrm{r},0} = 2.65\mathrm{m/s}$.

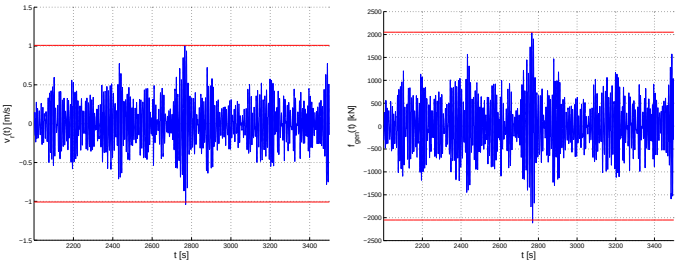

(a) (b)

Fig. 4: (a) Relative velocity $v_{\mathrm{r}}(t)$ and (b) generator loading $f_{\mathrm{gen}}(t)$ - time series representation when passive loading control strategy is applied for a JONSWAP spectrum defined by $H_{\mathrm{s}} = 3\mathrm{m}$ and $T_{\mathrm{p}} = 8.5\mathrm{s}$. Maximum expected amplitude are drawn in red solid lines, $\bar{v}_{\mathrm{r,Max}} = 1\mathrm{m/s}$, $\bar{f}_{\mathrm{gen,Max}} = 2050\mathrm{kN}$.

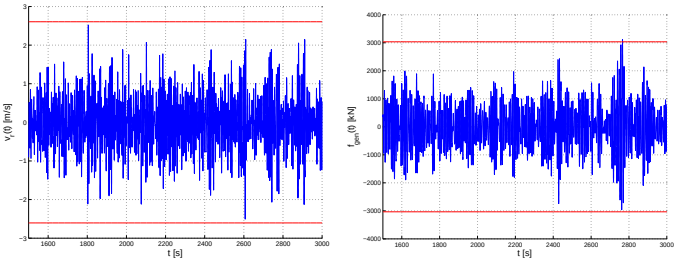

(a) (b)

Fig. 5: (a) Relative velocity $v_{\mathrm{r}}(t)$ and (b) generator loading $f_{\mathrm{gen}}(t)$ - time series representation when reactive loading control strategy is applied for a JONSWAP spectrum defined by $H_{\mathrm{s}} = 3\mathrm{m}$ and $T_{\mathrm{p}} = 8.5\mathrm{s}$. Maximum expected amplitude are drawn in red solid lines, $\bar{v}_{\mathrm{r,Max}} = 2.6\mathrm{m/s}$, $\bar{f}_{\mathrm{gen,Max}} = 3034\mathrm{kN}$.

B. *Long-term local wave climate analysis*

In offshore and wave energy community, long-term local wave climate analysis is traditionally performed on scatter diagram that represents sea-state occurrence frequency in term of joints significant wave height H_{s} and corresponding

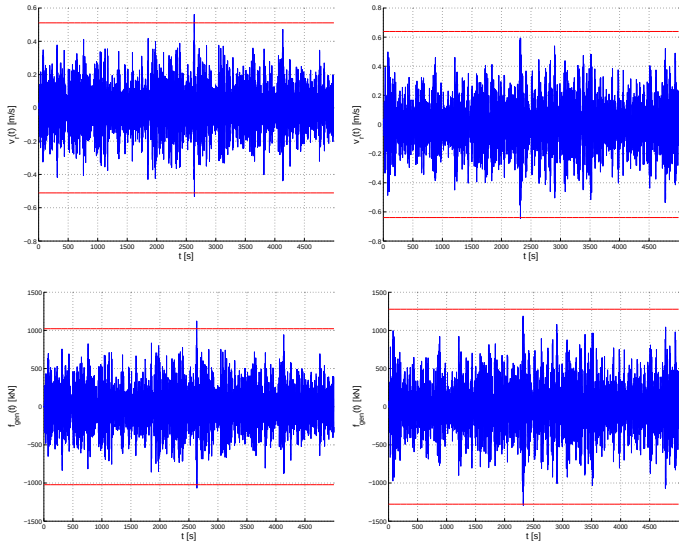

$(H_\mathrm{s}; T_\mathrm{p}) = (2; 6.5)$ $(H_\mathrm{s}; T_\mathrm{p}) = (2; 7.5)$

Fig. 6: Time series representation of the relative velocity and generator loading for different JONSWAP spectrum peak periods when passive loading control strategy is applied and no constraints are considered.

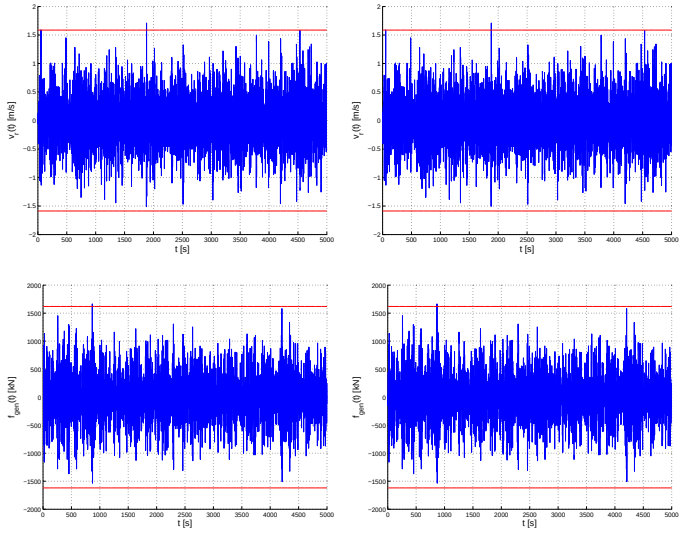

$(H_\mathrm{s}; T_\mathrm{p}) = (2; 9.5)$ $(H_\mathrm{s}; T_\mathrm{p}) = (2; 10.5)$

Fig. 7: Time series representation of the relative velocity and generator loading for different JONSWAP spectrum peak periods when MPC strategy is applied and no constraints are considered.

wave period (see for example [21]). Thereafter and to be consistent with the rest of the paper, spectrum peak period T_p will be adopted. Figure 8 illustrates the wave climate for a site localised near the Ushant island at coordinates $48°30'\mathrm{N} - 5°45'\mathrm{W}$. Data are provided by CANDHIS database (campaign 02902 - *Ouessant Large*) [22]. Data are arranged in regular spaced of $1\mathrm{m}$ bins for significant wave height and $1.2\mathrm{s}$ for peak period. The range of H_s is from $1\mathrm{m}$ to $13\mathrm{m}$ and T_p is from $1.2\mathrm{s}$ to $20.4\mathrm{s}$. In this study, we are not really interested to know if the site is adapted to the WEC but rather on the methodology for constraint pre-design. In what follows, we will use this scatter diagram as a reference site for numerical investigation. However regarding sampling used for drawing the scatter diagram, it will be convenient to

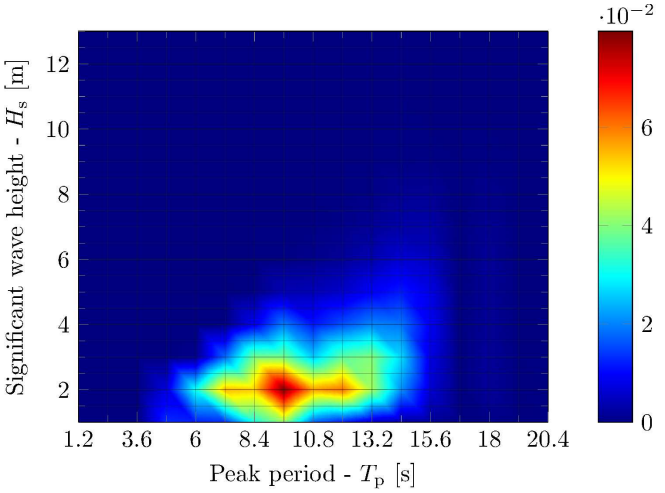

Fig. 8: Scatter diagram for the Ushant island site.

use an analytical representation of the data distribution. Such analytical functions are traditionally used for predicting the extreme values with a return period (20, 100 years and more) that should appeared on an offshore structure [20].

Several approaches can be used for modelling the long-term joint distribution $(H_\mathrm{s} - T_\mathrm{p})$ [23]. Herein, we adopt a bivariate distribution model constructed from two log normal distributions. One is for the significant wave height marginal distribution $f_{H_\mathrm{s}}(H_\mathrm{s})$ and the other for the peak period conditional distribution $f_{T_\mathrm{p}|H_\mathrm{s}}(T_\mathrm{p}|H_\mathrm{s})$. Identification procedure is quite simple and have been performed following [24] and [25]. Long-term joint distribution in terms of H_s and T_p (27) is the product of the marginal distribution with the conditional one.

$$f_{H_\mathrm{s}|T_\mathrm{p}}(H_\mathrm{s}, T_\mathrm{p}) = f_{H_\mathrm{s}}(H_\mathrm{s}) f_{H_\mathrm{s}|T_\mathrm{p}}(H_\mathrm{s}|T_\mathrm{p}) \qquad (27)$$

From this long-term statistical analysis, we are now able to perform a higher resolution study of short-term expected value and to estimate the average yearly power production. Here, if no constraint are taken into account, we estimate the average yearly power production to be $56.4\mathrm{kW}$ and $99.4\mathrm{kW}$, respectively for the passive and reactive control discussed previously, with the original scatter diagram. If evaluating it with a re-sampling scatter diagram (we used an increment of $.2\mathrm{m}$ for H_s and $.2\mathrm{s}$ for T_p), we find respectively $56.9\mathrm{kW}$ and $100.7\mathrm{kW}$, which is quite similar ($.88\%$ and 1.38% of difference).

It has to be mentioned that all the statistical analysis could be largely improved using for example a *Lonowe* model for the marginal distribution like in [24], [25], but this is out of the paper topic and for explaining the pre-design methodology we think it is good enough (according to the average yearly power production error).

C. Long-term maximum expected amplitude analysis

As a first approach, in the constraint process, two solutions could be envisaged:

- the use of extreme sea-state conditions, as it is done in offshore engineering,
- the use of maximum amplitudes (relative velocity and generator loading) that allow us to absorbed a certain percentage (or even 100%) of the total energy contained on the site; in other words maximising the harnessed

energy. Naturally, this last point could be investigated according to the control strategy.

We clearly understand that the first approach will be adopted for designing the WEC structure but it is not adapted for sizing the power electronic conversion chain. Indeed, it will oversize the conversion chain for only working, at its nominal rate, few times in its life. What about the second point? Figures 9 and 10 represent average yearly absorbed power distribution, when passive and reactive control is applied and no constraints are considered. The quantity is given in terms of maximum expected relative velocity (b) and generator loading (c). For both of them, we also represent the same quantity in term of maximum expected relative velocity when the system risks to be uncontrolled (a). In both cases, maximum relative velocity has been arranged in regular spaced of $.1\ \mathrm{m/s}$ bins and maximum generator loading have been arranged in regular spaced of $100\ \mathrm{kN}$ bins. The first point to notice is that, as expected, both maximum amplitudes are much higher when optimal control strategy is applied. Considering passive strategy most of the energy could be harnessed with a PTO that allows relative velocity around $1.8\mathrm{m/s}$ and a linear force around $8\mathrm{MN}$. On the other hand, considering optimal strategy, most of the energy could be harnessed with a PTO that allows relative velocity around $6\mathrm{m/s}$ and a linear force around $30\mathrm{MN}$. Don't forget that, as already mentioned in section I, fixing nominal velocity and force will fix the nominal power rating. That means that a $14.4\mathrm{MW}$ and a $180\mathrm{MW}$ generator will be required respectively in the first and second case. Presented like this, we well understand why the system have to be definitively constrained.

So, in this study we propose to constraint the system doing a mix between this two approaches. The whole procedure is performed considering a "nominal" working conditions. By "nominal", we mean in term of wave climate. We start first by constraining the system in term of relative velocity. Indeed, speaking in term of system consideration, the relative velocity is a system output. Then it is a result of the adopted control strategy and not a control variable. That also means that if the system is uncontrolled for a while (without necessary thinking about extreme conditions), it should be able to handle the appearing conditions. This is also one of the two reasons explaining why the nominal relative velocity have to be chosen based on an uncontrolled strategy. The second reason is much more related to the control strategy itself. Indeed, the wave excitation force is also a system input, or let say a perturbation. By constraining the generator loading we can not guaranty that the relative velocity is a consequence of our control strategy or of the perturbation because both of them are of the same level. This is well illustrated considering a passive control strategy. Figure 11 shows numerical results when a simple saturation is applied on the generator loading. Here a $480\mathrm{kN}$ have been considered that corresponds to a $2.4\mathrm{MW}$ nominal generator power rating with a $5\mathrm{m/s}$ nominal velocity. Obviously, it is clear that, in that particular case study, the wave excitation force dominates and drives the system. Indeed because of the quite high saturation, the WEC behaves like if it was freely-moving.

From this analysis we therefore recommend that the nominal relative velocity should be chosen based on the maximum expected relative velocity analysis when uncontrolled and in such a way that it allow us to absorb the maximum of the energy contained in the site. For example, here for the considered site, and from Fig. 9 (a) or 10 (a), a $5\mathrm{m/s}$ velocity could be a good candidate.

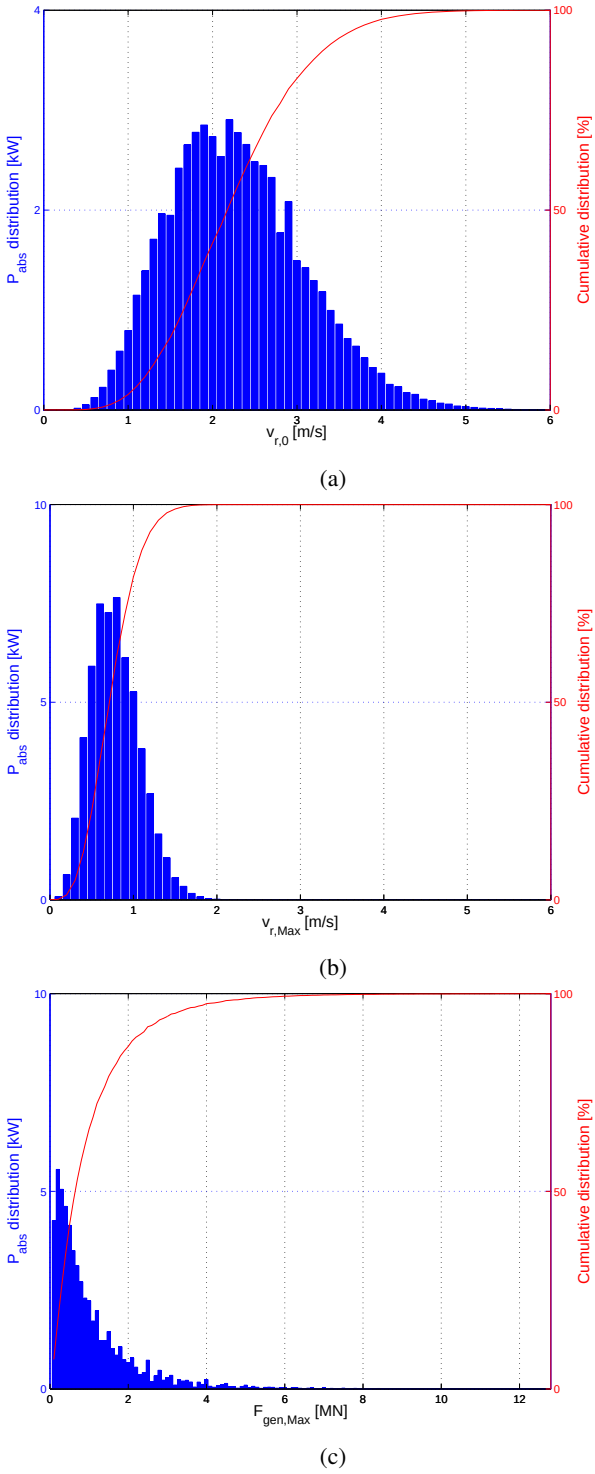

Fig. 9: Averaged power distribution, for passive control strategy, expressed in term of (a) $\bar{v}_{\mathrm{r},0}$, (b) $\bar{v}_{\mathrm{r,Max}}$ and, (c) $\bar{f}_{\mathrm{gen,Max}}$.

Remark: *For the rare cases where the relative velocity is higher than* $5\mathrm{m/s}$*, the WEC is put in safe mode (for example the power electronics are disconnected from the generator) and the system does not produce electricity anymore. From the cumulative distribution of Figs. 9(a) and 10(a), it is clear that it will have no impact on the annual power production.*

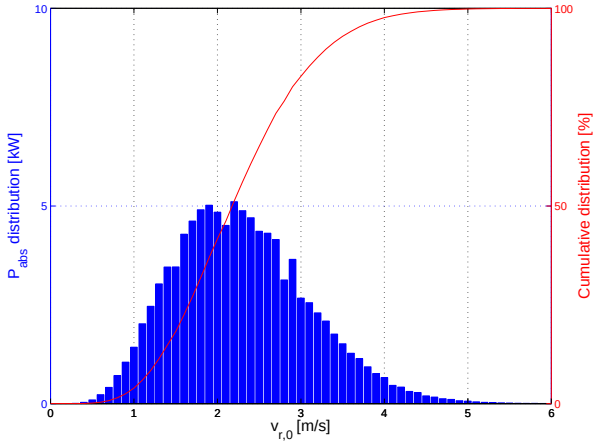

(a)

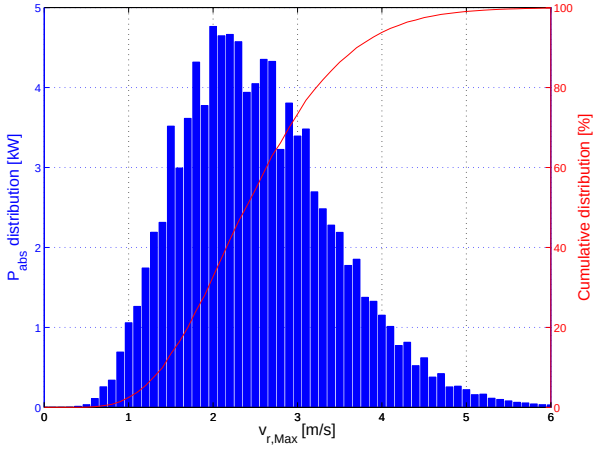

(b)

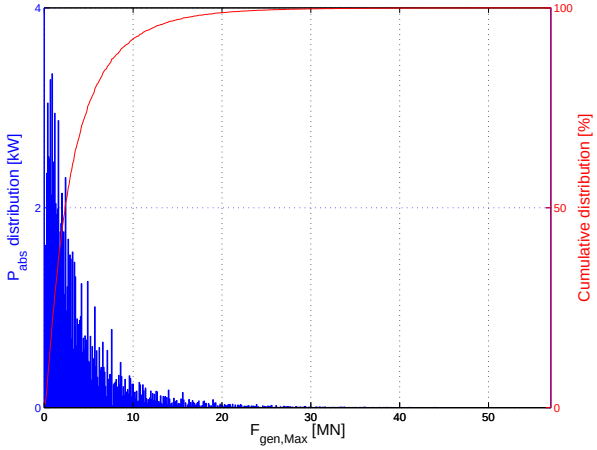

(c)

Fig. 10: Averaged power distribution, for optimal control strategy, expressed in term of (a) $\bar{v}_{\mathrm{r},0}$ (b) $\bar{v}_{\mathrm{r,Max}}$ and, (c) $\bar{f}_{\mathrm{gen,Max}}$.

In the next section we will discuss how to select the nominal generator power rating once the nominal velocity have been chosen.

V. Nominal Generator Power Rating Constraint

Now we have constrained the maximum relative velocity we may focus on the generator nominal power rating that will set the constraint on the control input. Because the proposed control strategy in section III is an optimal formulation, in what follows, we will size the generator power rating for that control strategy. However all the method is still valid

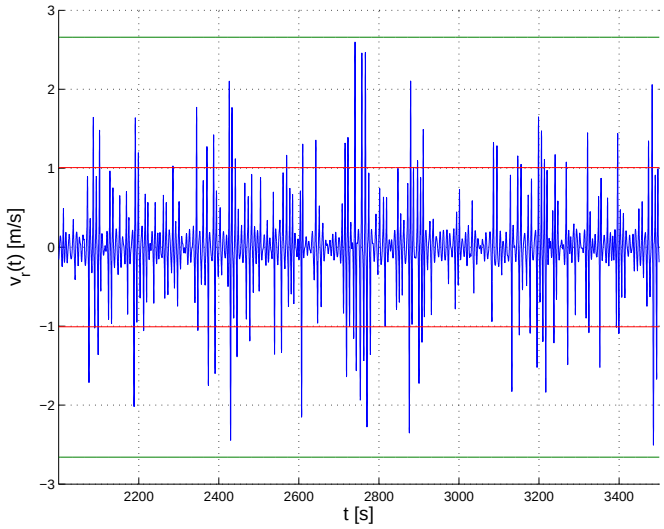

Fig. 11: Relative velocity $v_{\mathrm{r}}(t)$ time series representation when the system is passively controlled and for a JONSWAP spectrum defined by $H_{\mathrm{s}} = 3\mathrm{m}$ and $T_{\mathrm{p}} = 8.5\mathrm{s}$. Maximum expected amplitude when uncontrolled and controlled are respectively drawn in green and red solid line, $\bar{v}_{\mathrm{r},0} = 2.65\mathrm{m/s}$ and $\bar{v}_{\mathrm{r,Max}} = 1\mathrm{m/s}$.

for other control strategies as long as they ensure a generator loading constraint. Moreover, because the rest of the sizing procedure requires time-domain simulation and then it is quite cumbersome to guaranty convergence to the steady state, we will present all the procedure at a chosen spectrum. Here we decide to size the generator power rating for the couple $(H_{\mathrm{s}},\, T_{\mathrm{p}})$ that produces the maximum average power *i.e.* for $H_{\mathrm{s}} = 2.5\mathrm{m}$ and $T_{\mathrm{p}} = 9\mathrm{s}$.

The constraint procedure is quite simple. For the given spectrum, we perform several simulations for different nominal generator power rating values, P_{nom}, considering the control input constraint $F_{\mathrm{gen,Max}} = P_{\mathrm{nom}}/v_{\mathrm{r,nom}}$. For each simulation, we measure the average harnessed power P_{avg} and then we are able to evaluate two criteria defined as

- the maximisation of the produced electrical energy

$$c_1(P_{\mathrm{nom}}) = \frac{P_{\mathrm{avg}}}{P_{\mathrm{abs}}} \tag{28}$$

- the maximisation of the annual profit

$$c_2(P_{\mathrm{nom}}) = \alpha \frac{P_{\mathrm{avg}}}{P_{\mathrm{nom}}} \tag{29}$$

where P_{abs} is the average power that could be harnessed if no constraints are considered. Both criteria are normalized to unity to be comparable. So the second criterion has to be normalised using a scaling factor defined as $\alpha = \max(\frac{P_{\mathrm{avg},i}}{P_{\mathrm{nom},i}})$ where indice i denotes a sample. The first criterion c_1 measures the efficiency of the energy conversion chain without financial consideration that is introduce through the latter criterion c_2. This second criterion measures in a simple manner the economical efficiency of the energy conversion chain assuming, for sake of simplicity, that the installation cost is directly related to the nominal power rating of the installed generator. Figure 12 shows numerical results for the normalised criteria. Green and blue markers represent respectively c_1 and c_2 efficiency measures for several P_{nom}. It appears that data behave respectively as a hyperbolic tangent

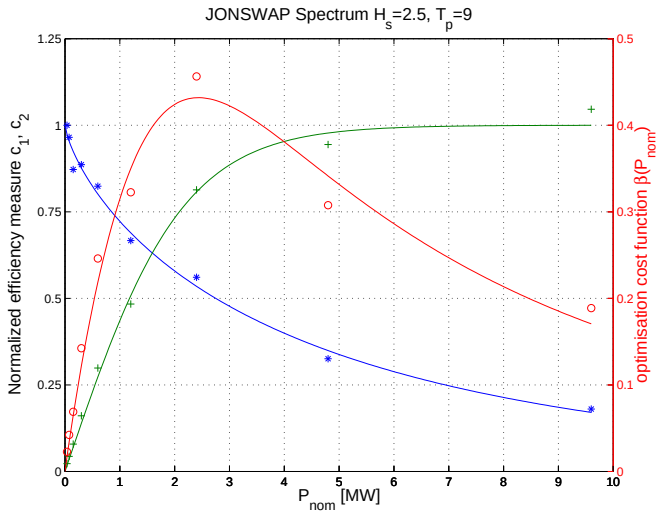

Fig. 12: Nominal generator power rating constraint process. Measure (marks) and fitted (solid line) data for the two efficiency criteria (conversion efficiency c_1 in green and economical criterion c_2 in blue). Optimisation cost function $\beta(P_{\mathrm{nom}})$ of the maximisation problem is represented in red. Optimal generator power rating $P_{\mathrm{nom,opt}} = 2.4\mathrm{MW}$.

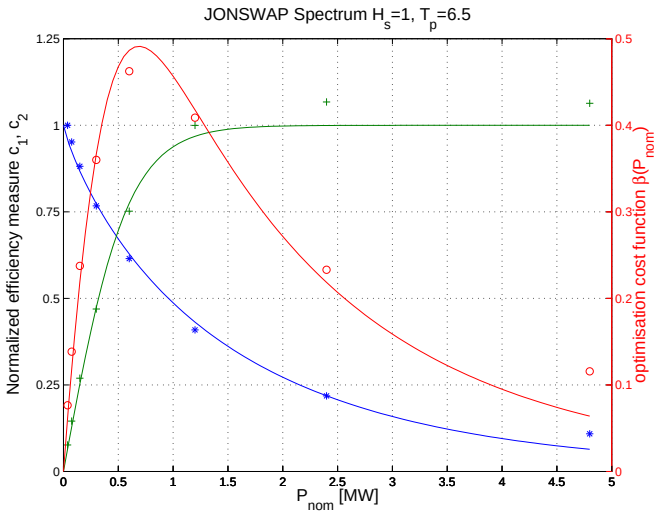

Fig. 13: Nominal generator power rating constraint process. JONSWAP spectrum - $H_{\mathrm{s}} = 1\mathrm{m}$, $T_{\mathrm{p}} = 6.5\mathrm{s}$. Optimal generator power rating $P_{\mathrm{nom,opt}} = 700\mathrm{kW}$.

and an exponential laws.

$$c_1(x) = \tanh(a_1 x) \tag{30}$$

$$c_2(x) = \exp(a_2 x^{b_2}) \tag{31}$$

where coefficients a_1, a_2, b_2 have to be identified. In this study, they have been fitted using a non-linear least square method. Obtained results are represented on the figure with green and blue solid line curves.

Based on this two criteria, we can define a maximisation problem searching for the higher produced electrical energy efficiency subject to the annual profit penalty function. Mathematically, this is an optimisation problem which is simply formulated through the maximisation of the cost function $\beta(P_{\mathrm{nom}})$ defined as the two criteria product.

$$\beta(P_{\mathrm{nom}}) = c_1(P_{\mathrm{nom}}) \times c_2(P_{\mathrm{nom}}) \tag{32}$$

This cost function should define an optimal generator power rating $P_{\mathrm{nom,opt}}$, that makes a compromise between a high power efficiency for the lower price. The cost function is drawn in red color on Fig. 12. Obviously it exists an optimal point (maximum) around $P_{\mathrm{nom}} = 2.4\mathrm{MW}$. Figure 13 shows numerical results for an other JONSWAP spectrum parametrised with ($H_{\mathrm{s}} = 1\mathrm{m}$ - $T_{\mathrm{p}} = 6.5\mathrm{s}$).

VI. Conclusions and Perspectives

In this paper, we have presented a simple method for predesigning the standard energy conversion chain of a wave energy converter. This was performed in a realistic fashion based on a known local wave climate. We proposed firstly to constraint the nominal generator velocity. From numerical investigations it have been shown that it have to be done based on the uncontrolled WEC behaviour. Once this latter have been defined, we can search for constraining the nominal generator power rating using time-domain simulation and then define the maximum control input limit. Several values are inspected and a simple optimisation procedure based on two antinomic criteria is proposed. The first criterion is based on the maximisation of the produced electrical energy and the second on the maximisation of the annual profit. Because all the procedure is quite time-cumbersome, we only present numerical results for the spectrum that produced the maximum yearly average power for the Ushant island selected site. It appears that it exist an optimal nominal generator power rating that makes a compromise between the two antinomic criteria. We well understand that this simple procedure could be applied on the whole scatter diagram and then it could be really easy to find the generator power rating based on the maximisation of criterion β over the whole scatter diagram. Also we have analysed the power generator constraint for an optimal control strategy but clearly all the procedure could be applied considering others strategies. Finally the procedure could be largely improved considering losses (mechanical, generator and power converters).

VII. Acknowledgment

This work was supported in part by the Fonds Unique Interministériel (France) – Project “EM Bilboquet”, in part by Région Bretagne, and in part by Conseil Général du Finistère.

References

[1] H. Titah-Benbouzid and M. Benbouzid, “Ocean wave energy extraction: Up-to-date technologies review and evaluation,” in *2014 International Power Electronics and Application Conference and Exposition*. IEEE, Nov. 2014, pp. 338–342.

[2] A. F. d. O. Falcão, “Wave energy utilization: A review of the technologies,” *Renewable and Sustainable Energy Reviews*, vol. 14, no. 3, pp. 899–918, Apr. 2010.

[3] J. Hals, J. Falnes, and T. Moan, “Constrained Optimal Control of a Heaving Buoy Wave-Energy Converter,” *Journal of Offshore Mechanics and Arctic Engineering*, vol. 133, no. 1, p. 11401, Nov. 2010.

[4] J. A. M. Cretel, G. Lightbody, G. P. Thomas, and A. W. Lewis, “Maximisation of Energy Capture by a Wave-Energy Point Absorber Using Model Predictive Control,” in *18th World Congress of the International Federation of Automatic Control (IFAC)*, vol. 18, no. 1, Milano, Italy, Aug. 2011, pp. 3714–3721.

[5] E. Abraham and E. C. Kerrigan, “Optimal Active Control and Optimization of a Wave Energy Converter,” *IEEE Transactions on Sustainable Energy*, vol. 4, no. 2, pp. 324–332, Apr. 2013.

[6] S. Olaya, J.-M. Bourgeot, and M. E. H. Benbouzid, "Optimal Control For a Self-Reacting Point Absorber: A One-Body Equivalent Model Approach," in *International Power Electronics and Application Conference and Exposition 2014 (IEEE PEAC'2014)*, Shanghai, China, 2014, pp. 332–337.

[7] A. O. Falcão and R. Rodrigues, "Stochastic modelling of OWC wave power plant performance," *Applied Ocean Research*, vol. 24, no. 2, pp. 59–71, Apr. 2002.

[8] E. Tedeschi, M. Carraro, M. Molinas, and P. Mattavelli, "Effect of Control Strategies and Power Take-Off Efficiency on the Power Capture From Sea Waves," *IEEE Transactions on Energy Conversion*, vol. 26, no. 4, pp. 1088–1098, Dec. 2011.

[9] S. Djebarri, J. F. Charpentier, F. Scuiller, and M. Benbouzid, "A systemic design methodology of PM generators for fixed-pitch marine current turbines," in *2014 First International Conference on Green Energy ICGE 2014*. IEEE, Mar. 2014, pp. 32–37.

[10] Ocean Power Technologies, "OPT PB150 PowerBuoy - Utility Power from Ocean Waves," pp. 0–1.

[11] Z. Yu and J. Falnes, "State-space modelling of a vertical cylinder in heave," *Applied Ocean Research*, vol. 17, no. 5, pp. 265–275, 1995.

[12] W. Cummins, "The impulse response function and ship motion," Tech. Rep., 1962.

[13] S. Olaya, J.-M. Bourgeot, and M. Benbouzid, "Modelling and Preliminary Studies for a Self-Reacting Point Absorber WEC," in *International Conference on Green Energy 2014 (ICGE'2014)*, Sfax, Tunisa, Mar. 2014, pp. 14–19.

[14] T. Perez and T. I. Fossen, "A Matlab Toolbox for Parametric Identification of Radiation-Force Models of Ships and Offshore Structures," *Modeling, Identification and Control: A Norwegian Research Bulletin*, vol. 30, no. 1, pp. 1–15, 2009.

[15] J. Falnes, "On non-causal impulse response functions related to propagating water waves," *Applied Ocean Research*, vol. 17, no. 6, pp. 379–389, Dec. 1995.

[16] S. Olaya, J.-M. Bourgeot, and M. Benbouzid, "Hydrodynamic Coefficient Computation for a Partially Submerged Wave Energy Converter," *IEEE Journal of Oceanic Engineering*, pp. 1–15 (in press), 2014.

[17] J. Falnes, "Wave-Energy Conversion Through Relative Motion Between Two Single-Mode Oscillating Bodies," *Journal of Offshore Mechanics and Arctic Engineering*, vol. 121, no. 1, pp. 32–38, Feb. 1999.

[18] J. Falnes, *Ocean Waves and Oscillating Systems - Linear Interactions Including Wave-Energy Extraction*. Cambridge University Press, Apr. 2002.

[19] Z. Yu and J. Falnes, "State-space modelling of a vertical cylinder in heave," *Applied Ocean Research*, vol. 17, no. 5, pp. 265–275, Oct. 1995.

[20] B. Molin, *Hydrodynamique des structures offshore - Guides pratiques sur les ouvrages en mer, in French*. Technip, 2002.

[21] A. Babarit, J. Hals, M. Muliawan, A. Kurniawan, T. Moan, and J. Krokstad, "Numerical benchmarking study of a selection of wave energy converters," *Renewable Energy*, vol. 41, pp. 44–63, May 2012.

[22] "http://candhis.cetmef.developpement-durable.gouv.fr/."

[23] A. Repko, "Uni-and bivariate statistical analysis of long-term wave climates," 1998.

[24] S. Haver, "Wave climate off northern Norway," *Applied Ocean Research*, vol. 7, no. 2, pp. 85–92, Apr. 1985.

[25] T. Moan, Z. Gao, and E. Ayala-Uraga, "Uncertainty of wave-induced response of marine structures due to long-term variation of extratropical wave conditions," *Marine Structures*, vol. 18, no. 4, pp. 359–382, May 2005.